J. Engg. Math., 16, 325–347 (1982). 0022–0833/82/04/0325–23 $00.20/0

The Oseen model for internal separated flows

S. V. RAMAKRISHNAN and P. N. SHANKAR

Aerodynamics Division, National Aeronautical Laboratory, Bangalore-560 037, India

(Received December 1, 1981)

SUMMARY

The flow field studied in this paper is the viscous laminar, separated flow downstream of a sudden expansion in a two-dimensional duct. The flow is modelled by the Oseen equations and a solution is sought for the downstream flow given the conditions at the sudden expansion. First, the exact solution to a high-Reynolds-number limit equation suggested by Kumar and Yajnik [6] is obtained. Next, the solution to the full equations is sought in terms of an eigenfunction-expansion procedure which leads to a non-standard eigenvalue problem. A detailed study is made of the latter and a number of expansion procedures are considered for the boundary-value problem. Specific calculations of the separated flow are presented for Reynolds numbers $R = 10^n, n =$ 0–5. It is found that as $R \to \infty$ the solution of the full equation does indeed agree with the solution of the high-Reynolds-number limit equation. In particular it is found that the length of the recirculating region x_r scales with R as $R \to \infty$.

1. Introduction

The Oseen equations have traditionally been used as approximate equations for low-Reynolds-number flows past bodies. They are also known to be a valid approximation to the Navier-Stokes equations for high-Reynolds-number flows at large distances from finite bodies [1]. On the other hand, one can look at the linear Oseen equations as model equations to study the gross features of viscous flows at all Reynolds numbers. From this point of view, the aim is not to get accurate solutions for real viscous flows; rather it is to get the qualitative features of such flows and to gain experience on the problems associated with the full Navier-Stokes equations. This approach is especially useful when studying certain difficult flow problems. We use this approach here to study internal separated flows.

The idea of using the Oseen equations as model equations for high Reynolds numbers goes back to Oseen himself [2], who obtained general results concerning external separated flows past finite bodies. Since then there have been a number of papers concerned with external separated flows past finite two-dimensional bodies as modelled by the Oseen equations; one can refer to Kusukawa [3] and Miyagi [4] and to the references quoted therein for the more recent work on the subject. However, there appear to be few applications, if any, of the model equations to internal separated flows. As internal separated flows are laterally bounded, they are in some ways conceptually simpler than external flows. It would, therefore, seem profitable to study such flows using the model equations, since the analysis should be simpler. As will be

shown this is indeed so, but the mathematical problems are still non-trivial as they lead to a non-standard eigenvalue problem.

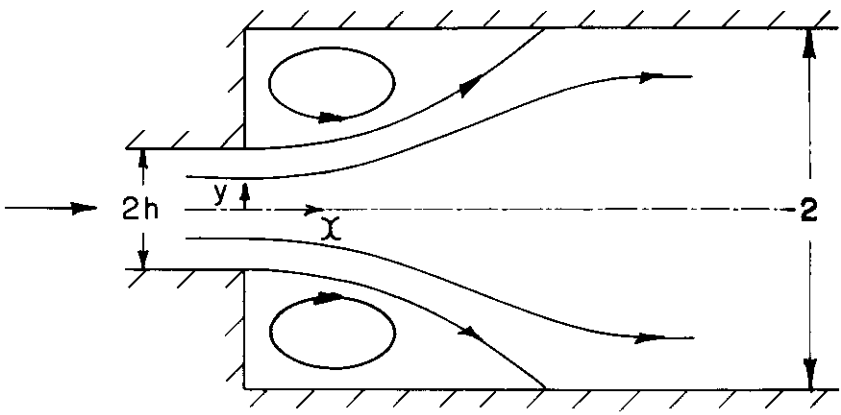

Figure 1. The sudden expansion in a duct.

The specific geometry considered is that of a sudden expansion in an infinite two-dimensional, straight duct (Figure 1). It is assumed that the flow (e.g. the fluid-velocity field) is known at the sudden expansion with the calculation of the downstream separated flow as the objective. The flow is assumed steady, laminar and two-dimensional. The corresponding problem for the Navier-Stokes equations has been considered, among others, by Hung and Macagno [5], who use a numerical finite-difference method and are limited in Reynolds number, and by Kumar and Yajnik [6], who derive and use a boundary-layer-like limit equation for high Reynolds numbers. The present work, we believe, by virtue of its analytical simplicity, sheds light on these studies.

The main results of this paper are: (i) The nature of the separated flow at a sudden expansion is elucidated through the use of the model equations. In particular it is shown that the length of the recirculating region increases linearly with Reynolds number as this parameter tends to infinity. (ii) By solving exactly a high-Reynolds-number limit equation the nature of the solution considered by Kumar and Yajnik [6] is clarified. Moreover, in the present case the solution of the full equations is shown to agree, in the limit $R \to \infty$ with the solution of the limit equation. This lends support to the use of such limit equations for internal separated flows at high Reynolds numbers. (iii) A non-standard eigenvalue problem is studied in some detail. Apart from the physical interest of the separated flow solutions, the eigenvalue problem merits interest on its own.

2. Formulation

We consider the flow of a viscous fluid at a sudden expansion in a two-dimensional straight duct assuming the flow to be incompressible, steady and two-dimensional. The velocity field far

downstream will naturally correspond to Poiseuille flow in the duct. Let all lengths be normalised by the duct half-width a, velocities by the mean velocity U of the Poiseuille flow and pressure by ρU^2, where ρ is the density of the fluid. Then the model equations to be used take the form

$$u_x + v_y = 0, \tag{1.1}$$

$$u_x = -p_x + R^{-1} \nabla^2 u, \tag{1.2}$$

$$v_x = -p_y + R^{-1} \nabla^2 v, \tag{1.3}$$

where $R = aU/\nu$ is the Reynolds number.

As for conditions at the duct expansion, one could consider a number of alternate conditions. Here we choose to prescribe the initial velocity profile

$$\left.\begin{aligned} u(0, y) &= u_0(y) \\ v(0, y) &= v_0(y) \end{aligned}\right\} \quad \text{on } -1 \leqslant y \leqslant 1 \tag{2.1, 2.2}$$

The other boundary conditions are the no-slip condition at the duct walls and the x-independent velocity-field requirement far downstream

$$u(x, \pm 1) = v(x, \pm 1) = 0; \tag{3.1}$$

$$u_x \to 0, \qquad v \to 0 \qquad \text{as} \qquad x \to \infty. \tag{3.2}$$

Since the fluid is incompressible, one can use a stream function Ψ which satisfies the equation

$$\nabla^2 \left(\nabla^2 - R \frac{\partial}{\partial x} \right) \Psi = 0. \tag{4}$$

This is the basic governing equation used. At the risk of repetition it might be worthwhile to clarify once again the nature of the approximation used and the point of view taken here. It is clear that since all the non-linear terms of the Navier-Stokes equation have been dropped or replaced by linear ones, the model equations may well miss certain features contained in the solutions of the N-S equation. Further, the use of the mean velocity as the constant in the x-convection term, though reasonable, might be questioned; one could consider replacing the terms u_x and v_x in (1.2) and (1.3) by cu_x and cv_x and choosing c 'appropriately'. The latter could easily be done, but this would not change the essential features of interest. Thus, in a sense the choice of the model equations has been based on convenience. On the other hand, it is very likely that when $R \to 0$ the model equations are a good approximation to the N-S equation; so too if the ratio of the duct entry to the duct width is close to unity, and the initial velocity profile is uniform. In any case, the point of view taken here is that the model equations are the simplest ones to study and are likely to reveal interesting features of the separated flow in the duct.

3. An approximate solution for high Reynolds numbers

Although the boundary value problem posed in Section 2 is linear, it turns out, as will be shown in Section 4, that it is not easy to solve it explicitly to obtain useful qualitative or quantitative results. We shall therefore first consider here an approximation for high Reynolds numbers i.e. for $R \to \infty$.

We follow here the ideas of Kumar and Yajnik who argue that for $R \to \infty$ the relevant length scales for the calculation of the downstream flow are of order 1 and R in the transverse y direction and the streamwise x-direction respectively. Thus, in this approximation the relevant limit equation derived from the governing equation (4) is

$$\frac{\partial^2}{\partial y^2}\left(\frac{\partial^2}{\partial y^2} - R\,\frac{\partial}{\partial x}\right)\Psi = 0. \tag{5}$$

The above equation corresponds to equation (3) of Kumar and Yajnik. It is to be noted that while the approximation is indeed 'boundary-layer'-like in appearance, the governing ideas are not quite the same. This can be seen by going back to the equations (1) for the velocity field. It is true that in this approximation (1.3) implies that the pressure is constant across the duct and hence the y-component of velocity is now given by the continuity equation (1.1). However, unlike the external boundary-layer case, the pressure here is not known a priori nor is there the equivalent of a free-stream boundary condition; rather the lateral boundary conditions are at the duct walls alone.

As for the boundary conditions at $x = 0$, it is clear that since the highest x-derivatives have been lost, it will not be possible to satisfy both the conditions (2.1) and (2.2). This is not surprising as the arguments leading to the limit equation are not valid for small x, where a different limit equation is appropriate. Kumar and Yajnik assume without proof the very plausible matching condition

$$\lim_{x \to 0} \Psi(x, y) = \Psi_0(y). \tag{6}$$

This amounts to enforcing condition (2.1) alone on the streamwise component. It is clear that this solution cannot be valid for regions close to the duct enlargement, but presumably the approximations are reasonable for $x \sim R$. We too shall use (6) and show that the resulting solutions agree well with the exact solutions for large R.

The boundary-value problem constituted by (5) subject to the boundary conditions (6) and (3) can be easily solved either by using the Laplace transform or by using a duct-mode-expansion procedure. While we have used both as checks on one another, we present only the latter procedure as this method is then used in Section 4 for the full problem. It is easy to verify that the simply separable solutions of (5), which decay for $x \to \infty$, are of the type $f(y) \exp(-\lambda x)$, $(\mathrm{Re}\,\lambda > 0)$; assuming such modes, one finds that the full stream function $\Psi(x, y)$ is given by

$$\Psi(x, y) = \tfrac{3}{2} y - \tfrac{1}{2} y^3 + \psi(x, y), \tag{7}$$

where

$$\psi(x,y) = \sum_{n=1}^{\infty} a_n e^{-\frac{\xi_n^2 x}{R}} \left\{ y - \frac{\sin(\xi_n y)}{\sin \xi_n} \right\} + b_n e^{-\frac{n^2\pi^2 x}{R}} \left\{ 1 - \frac{\cos n\pi y}{\cos n\pi} \right\}, \tag{8.1}$$

$$a_n = -\frac{1}{\sin \xi_n} \int_{-1}^{1} \left\{ \Psi(0,y) - \tfrac{3}{2} y + \tfrac{1}{2} y^3 \right\} \sin(\xi_n y) dy, \tag{8.2}$$

$$b_n = -\cos n\pi \int_{-1}^{1} \left\{ \Psi(0,y) - \tfrac{3}{2} y + \tfrac{1}{2} y^3 \right\} \cos n\pi y dy. \tag{8.3}$$

In the above solution the eigenvalues ξ_n corresponding to the odd eigenfunctions are solutions of the equation

$$\tan \xi = \xi \tag{9}$$

which has only real roots. In this high-Reynolds-number approximation, therefore, the duct modes are all real and as (8.1) shows the final solution exhibits the relevant axial length as x/R showing the analysis to be consistent. The formulae for a_n and b_n are discussed in Section 4.2.

We observe that if the duct expansion and the inlet flow are symmetric the coefficients b_n in (8.1) vanish, and we need to use only the odd eigenfunctions. The calculations displayed in Figures 2 and 3 are for such symmetric flows. Figures 2a and 2b show the streamline patterns for a parabolic entry profile for duct expansion ratios of 2 and 10 respectively. These computations utilised the first 20 eigenvalues of (9) and were checked using 30 and 40 eigenvalues. It was found that 20 eigenvalues were sufficient for a 5 decimal place accuracy in Ψ. The streamline patterns computed are qualitatively similar to those obtained by Kumar and Yajnik and Hung and Macagno except for the fact that the separating streamline is here concave to the flow. However, there appear to be significant differences in the length of the recirculating region (x_r) and the maximum Ψ-values there (Ψ_e). For example, at an expansion ratio of 2, the present model yields a value of .017 for x_r/R and Ψ_e not sensibly different from 1.00000 (i.e. the recirculating region appears to be a dead water region); whereas, Kumar and Yajnik and Hung and Macagno get values around 0.065 and 1.05 for x_r and Ψ_e respectively. It is very likely that the large quantitative differences are due to the different models used; no doubt, the Oseen model grossly overestimates the axial convection and in the recirculating region even the direction might be wrong. On the other hand, it should be pointed out that Hung and Macagno's results are for a low Reynolds number (46.6) while Kumar and Yajnik used only 3 terms in their expansion procedure and had errors in their inlet velocity profile representation of the order of 0.1 in u. We shall show in Section 4, from the full solution for this model, that 46 is indeed a low Reynolds number for such comparisons. And as for accuracy the present calculations were based on 20 terms of the eigenfunction expansion, used double-precision arithmetic and the error on the initial-profile representation was of the order of 0.00001. Thus some caution must be exercised in quantitatively comparing the present results with those of the earlier investigations.

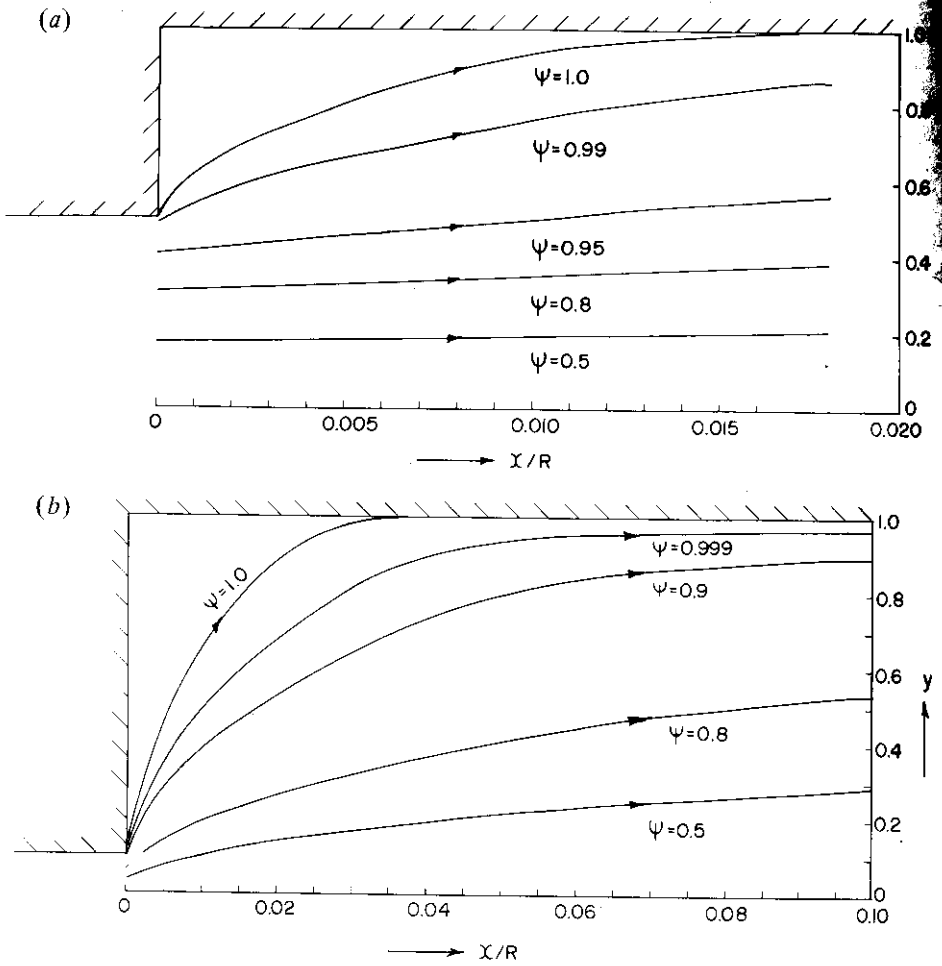

Figure 2a. The streamline pattern for an expansion ratio $(1/h) = 2$.
Figure 2b. The streamline pattern for an expansion ratio $(1/h) = 10$.

Figure 3 shows the variation of the length of the recirculating region, x_r, as a function of duct-entry half-width. Figure 4 shows the streamline pattern for a non-symmetric duct expansion with parabolic entry profile. It will be shown in the next section that the approximation for high Reynolds numbers used here leads to results in agreement with those obtained by the use of the full equations.

4. The solution of the full equations

We now consider the solution of the full boundary-value problem, valid for all R posed by equation (4) subject to the boundary conditions (2) and (3). For $R \neq 0$ the simply separable solutions of (4) which decay for $x \to \infty$ are of the form $\phi(y) \exp(-\lambda x)$; assuming such modes,

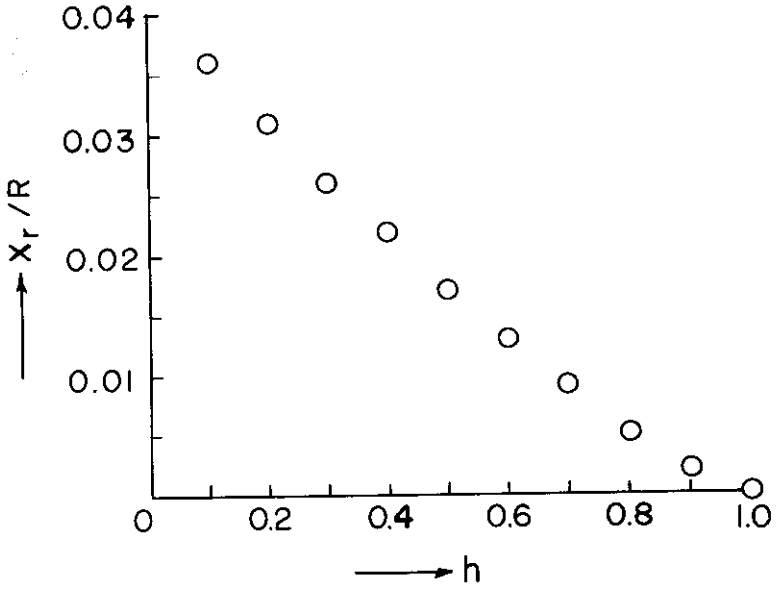

Figure 3. Variation of the length of the recirculating region x_r with h.

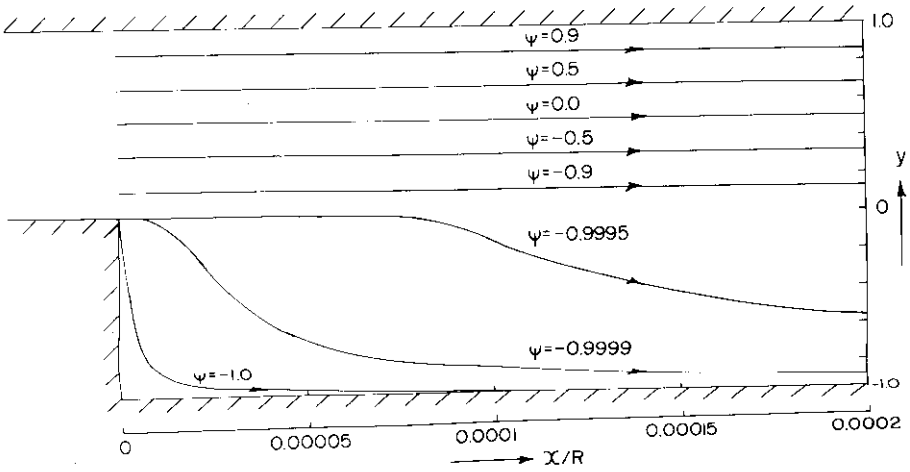

igure 4. Streamline pattern for an asymmetric expansion with parabolic entry profile.

ne is led to the generalised eigenvalue problem

$$\phi_{yyyy} + (2\lambda^2 + R\lambda)\phi_{yy} + \lambda^2(\lambda^2 + R\lambda)\phi = 0, \tag{10.1}$$

$$\phi(\pm 1) = \phi'(\pm 1) = 0. \tag{10.2}$$

ow, although the differential operator in (10.1) is formally self-adjoint, it depends on the neralised eigenvalue λ, which appears non-linearly in both coefficients. Thus, one cannot

hope to find only purely real eigenvalues. In fact, for $R = 0$ it is easy to show that all the eigenvalues are actually complex. Another serious difficulty is that since the eigenvalue appears in the operator, a simple expansion procedure based on orthogonality or biorthogonality is ruled out. Nevertheless, the great advantage of the present model is that since the equation has coefficients independent of y, the eigenvalue problem can be reduced to a transcendental equation. As the only solutions, for $R \neq 0$ of (10.1) are trigonometric, the eigenvalue problem reduces to the solution of

$$\tan \lambda/\lambda = \tan \sqrt{\lambda^2 + R\lambda} \,/\, \sqrt{\lambda^2 + R\lambda} \tag{11.1}$$

with corresponding eigenfunction

$$\phi(y) = \sin(\lambda y) - \frac{\sin \lambda}{\sin \sqrt{\lambda^2 + R\lambda}} \sin(\sqrt{\lambda^2 + R\lambda} \cdot y) \tag{11.2}$$

for a symmetric duct expansion, which is the only case to be considered here. The eigenvalue problem and the estimation of the flow development will be considered in turn.

4.1 The eigenvalue problem

In general (11.1) will admit complex eigenvalues. This is most easily seen by setting $R = 0$ in (4), corresponding to Stokes flow; the eigenvalue problem for modal solutions leads to the transcendental equation

$$\sin 2\lambda = 2\lambda \tag{12}$$

which is well known to have only complex roots. Since for small R the solutions of (12) should be a good first approximation to the solutions of (11.1), one would expect (11.1) in general to have complex roots.

Before looking at the general properties of the eigenvalues and the method of their computation, it is helpful to look at some plots of their distribution in the complex λ-plane. Figures 5a and 5b show the distribution of the lowest eigenvalues, ordered by the magnitudes of their real part, for Reynolds numbers of 1, 10, 100 and 1000. The first thirty eigenvalues for $R = 10^4$ and 10^5 are all real and hence are not shown. For $R = 1$ all the eigenvalues are complex while for $R = 1000$ there are only two complex eigenvalues in the range shown. One observes also that the eigenvalues (particularly the real ones) tend to crowd towards the origin as $R \to \infty$. Figure 6 shows the locus of a particular eigenvalue, namely the first at $R = 0$ as R increases from zero to 200. We might point out that the left-running real eigenvalues generated by the coalescence of complex conjugate pairs is not shown in this figure. Note particularly that the eigenvalue is purely real over finite ranges of the Reynolds number, e.g. between 8.55 and 10.3 and that the imaginary part keeps getting smaller.

We now list some analytic properties of the eigenvalues which are useful in determining them. (a) If λ is an eigenvalue, its conjugate is an eigenvalue. Since we are interested only in

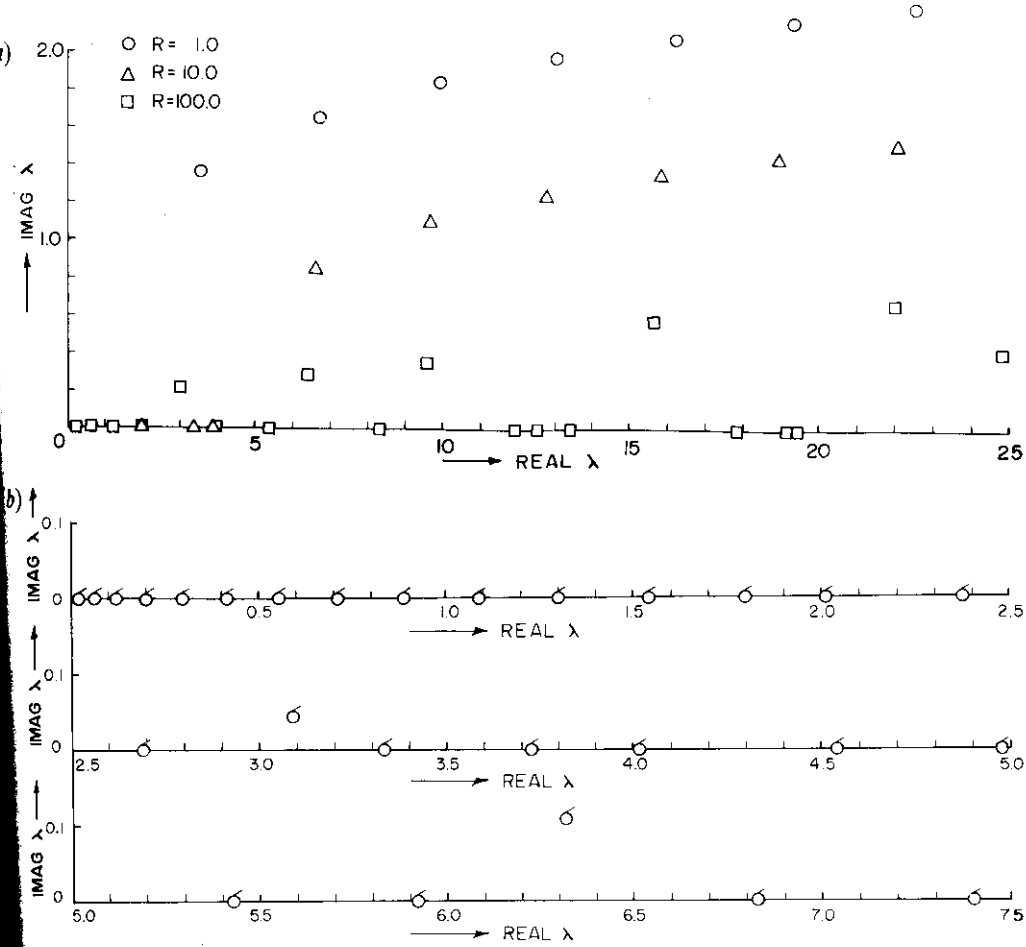

ure 5a. Distribution of eigenvalues with $\lambda_r > 0$, $\lambda_i \geqslant 0$ in the complex λ-plane. The complex conjugates also eigenvalues.

ure 5b. Distribution of the eigenvalues for $R = 1000$.

nded solutions, i.e. those with $\lambda_r > 0$, this restricts the search to the upper right half-plane ne. (b) Since $\lambda(= \lambda_r + i\lambda_i)$ is in general complex, it would be useful to have a bound on λ_i. tiplying (10.1) by the conjugate of ϕ and integrating over the interval one finds

$$\int |\phi''|^2 dy - (2\lambda^2 + R\lambda) \int |\phi'|^2 \, dy + \lambda^2(\lambda^2 + R\lambda) \int |\phi|^2 dy = 0.$$

ne now takes the imaginary part of the equation and assumes $\lambda_i > 0$ it is easy to conclude

$$\lambda_i \leqslant \lambda_r \left\{ \frac{4\lambda_r + 3R}{4\lambda_r + R} \right\}^{1/2} \tag{13}$$

is a useful bound because it restricts the search for complex eigenvalues essentially to a

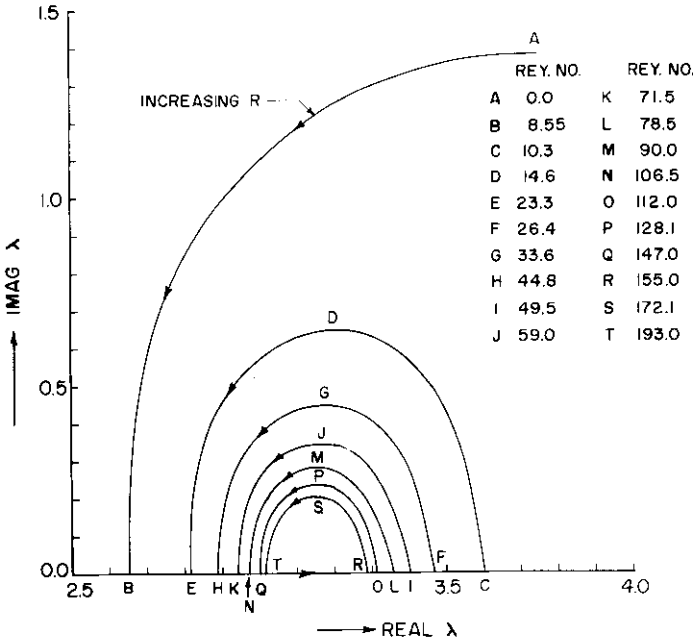

Figure 6. The locus of the first eigenvalue for $R = 0$ as R increases. Note that for ranges of values of R, e.g. between B–C, E–F etc., the eigenvalue is real.

wedge in the upper right half-plane. (c) Since the roots of (12) approximate those of (11.1) for $R \to 0$ and since (12) is known to have only complex roots with $\lambda_i \ll \lambda_r$ as $|\lambda| \to \infty$, it is natural to seek asymptotic solutions to (11.1) with $\lambda_r \sim (4n+1)\,\pi/4$, $\lambda_i \ll \lambda_r$, $R \ll \lambda_r$ for large integer n. Substituting these forms into (11.1) one finds the asymptotic solutions

$$\lambda_r \sim (4n+1)\,\frac{\pi}{4} - \left(\frac{R}{4} + \frac{\ln\{(4n+1)\pi\}}{(4n+1)\pi}\right), \tag{13.1}$$

$$\lambda_i \sim \tfrac{1}{2}\ln\{(4n+1)\pi\}. \tag{13.2}$$

This expansion for fixed R, $\lambda_r \to \infty$ leads to two conclusions. No matter how large R is, there will exist complex roots i.e. one cannot hope for a purely real spectrum even for large R. Secondly, consistent with the bound given by (13), (13.2) shows that the eigenvalues cannot be boxed in a strip of finite width in the plane. We note that (13.1) also indicates that for sufficiently large n the eigenvalues of this sequence should be spaced approximately π apart. This trend is evident in Figure 5a for the lower Reynolds numbers. (d) For $R \to \infty$, Figures 5a and 6 suggest the existence of roots of $O(1)$, and the figures further suggest that these lie in the neighbourhood of $n\pi$. This assumption leads to the asymptotic formulae for $R \to \infty$,

$$\lambda \sim n\pi\,(1 + \epsilon + \ldots.), \tag{14.1}$$

$$\epsilon_r = -\frac{2(\tan A - A/2)}{A(A\tan A + 1)}, \tag{14.2}$$

$$\epsilon_i^2 = \frac{2\{(1+\epsilon_r)\tan A - A\epsilon_r\}}{A(A\tan A + 1)}, \tag{14.3}$$

where $A = (n\pi R)^{1/2}(1 + \epsilon_r/2)$ and $n\pi \ll R$. This formula is unfortunately not explicit, but it would still be easier to compute an initial approximation for λ from the above rather than (11.1) as ϵ is small. (c) Finally the limit analysis for $R \to \infty$ of Section 3 suggests the likelihood of roots $\lambda \sim O(1/R)$ as $R \to \infty$. This assumption leads to the asymptotic formula for $R \to \infty$,

$$\lambda \sim \frac{\xi^2}{R} + \frac{\xi^3}{R^2}\frac{(1 - \sec^2\xi + \frac{2}{3}\xi^2)}{(\sec^2\xi - \xi)}, \tag{15}$$

where ξ satisfies $\tan\xi = \xi$. Thus as $R \to \infty$ the roots of (11.1) that are closest to the origin, i.e. the most important roots, correspond to those of (9), the eigenvalues of the limit equation used in Section 3. This already suggests the essential validity of the approximation in Section 3.

The properties of the eigenvalues listed above give the general impression that the spectrum has two distinct branches, a low-Reynolds-number one connected with the approximation (12), and a high-Reynolds-number branch related to the approximation (9). While this is partially true, careful computation shows that as R increases pairs of real eigenvalues are formed when complex conjugate pairs come together on the real axis; the resulting left-running ones then migrate to the neighbourhood of the origin provided they do not collide earlier with a right-running real eigenvalue. While the real eigenvalues near the origin dominate the flow for high Reynolds numbers, complex eigenvalues will always be present.

With this picture in hand, the location and accurate computation of the eigenvalues is not too hard. For a given R one hunts along the real axis for the real roots from the second branch whose location will be approximately given by (15). The (generally) complex roots from the first branch are found either by starting from the roots of (12) or from formula (13) and tracking them using Newton's method. Generally for any computation the first 30 eigenvalues, ordered by their real parts, were located.

It is possible at times to inadvertently miss roots, particularly complex ones with small imaginary parts. In order to guarantee that no roots have been missed in a given region of the λ-plane, it is most useful to apply the principle of the argument (see Dettman [7] for example). Some missing roots were actually located by the use of this theorem. Tables 1a and 1b list the first 25 roots of (11.1) for Reynolds numbers 10^n, $n = 0, 1, 2, 3, 4$. For $R = 10^5$ to this accuracy, the roots are given by multiplying those for $R = 10^4$ by 0.1.

4.2 *The solution of the duct-expansion problem*

The difficulty in using the eigenfunctions $\{\phi_n(y, \lambda_n), n = 1, 2, \ldots\}$ generated in Section 4.1 to solve the duct-expansion problem stems from the fact that there is no clear-cut expansion

Table 1a. The first 25 eigenvalues for $R = 1, 10, 100$.

	$R = 1$	$R = 10$	$R = 100$
1	$3.51591 + 1.36026\,i$	1.99794	0.20177
2	$3.51591 - 1.36026\,i$	3.36027	0.59567
3	$6.70989 + 1.65432\,i$	3.85030	1.18534
4	$6.70989 - 1.65432\,i$	$6.60710 + 0.83661\,i$	1.97645
5	$9.87624 + 1.83717\,i$	$6.60710 - 0.83661\,i$	$3.03480 + 0.22180\,i$
6	$9.87624 - 1.83717\,i$	$9.65423 + 1.08771\,i$	$3.03480 - 0.22180\,i$
7	$13.0327 + 1.97057\,i$	$9.65423 - 1.08771\,i$	3.93836
8	$13.0327 - 1.97057\,i$	$12.73150 + 1.24160\,i$	5.34325
9	$16.1843 + 2.07571\,i$	$12.73150 - 1.24160\,i$	$6.44093 + 0.29199\,i$
10	$16.1843 - 2.07571\,i$	$15.8269 + 1.35264\,i$	$6.44093 - 0.29199\,i$
11	$19.3331 + 2.16252\,i$	$15.8269 - 1.35264\,i$	8.29704
12	$19.3331 - 2.16252\,i$	$18.9339 + 1.43978\,i$	$9.61622 + 0.35087\,i$
13	$22.4802 + 2.23646\,i$	$18.9339 - 1.43978\,i$	$9.61622 - 0.35087\,i$
14	$22.4802 - 2.23646\,i$	$22.0488 + 1.51173\,i$	11.9325
15	$25.6262 + 2.30087\,i$	$22.0488 - 1.51173\,i$	12.4981
16	$25.6262 - 2.30087\,i$	$25.1690 + 1.57318\,i$	13.3867
17	$28.7713 + 2.35791\,i$	$25.1690 - 1.57318\,i$	$15.6381 + 0.56660\,i$
18	$28.7713 - 2.35791\,i$	$28.2933 + 1.62696\,i$	$15.6381 - 0.56660\,i$
19	$31.9159 + 2.40911\,i$	$28.2933 - 1.62696\,i$	17.7812
20	$31.9159 - 2.40911\,i$	$31.4205 + 1.67485\,i$	19.1060
21	$35.0600 + 2.45555\,i$	$31.4205 - 1.67485\,i$	19.3608
22	$35.0600 - 2.45555\,i$	$34.5499 + 1.71808\,i$	$21.9972 + 0.66624\,i$
23	$38.2037 + 2.49804\,i$	$34.5499 - 1.71808\,i$	$21.9972 - 0.66624\,i$
24	$38.2037 - 2.49804\,i$	$37.6812 + 1.75753\,i$	$24.7759 + 0.41873\,i$
25	$41.34714 + 2.55721\,i$	$37.6812 - 1.75753\,i$	$24.7759 - 0.41873\,i$

Table 1b. The first 25 eigenvalues for $R = 1000, 10{,}000$.

	$R = 1000$	$R = 10{,}000$
1	0.0201906	0.00201907
2.	0.0596781	0.00596795
3	0.1188939	0.0118900
4	0.1978448	0.0197858
5	0.2965255	0.0296554
6	0.4149337	0.0414989
7	0.5530670	0.0553164
8	0.7109220	0.0711077
9	0.8884983	0.0888729
10	1.0858003	0.1086119
11	1.3028426	0.1303249
12	1.5396589	0.1540117
13	1.7963325	0.1796724
14	2.0730625	0.207307
15	2.3704247	0.2369153
16	2.6908248	0.2684976
17	$3.0903088 + 0.0378163\,i$	0.3020536
18	$3.0903088 - 0.0378163\,i$	0.3375834
19	3.3332871	0.3750871
20	3.7278171	0.4145646
21	4.1251951	0.4560157
22	4.5400317	0.4994406
23	4.9744095	0.5448394
24	5.4304710	0.5922118
25	5.9198748	0.6415581

theorem to indicate how they are to be used to represent a given initial-velocity distribution at $x = 0$. It is easily verified that they are not an orthogonal set at least to any known weight; moreover, it is to be noted that two conditions have to be satisfied at $x = 0$, e.g. $\Psi(0, y)$ and $\Psi_x(0, y)$ might be prescribed.

It is worthwhile at this stage to compare this situation with that which occurred in the high-Reynolds-number approximation of Section 3. In that case if modal solutions of the form $\hat{\phi}(y) \times \exp(-\lambda x)$ were sought for the governing equation (5), the eigenfunctions had to satisfy

$$\frac{d^4\hat{\phi}}{dy^4} + R\lambda \frac{d^2\hat{\phi}}{dy^2} = 0 \tag{16}$$

subject to the no-slip condition at the side walls. Now, although (16) is not a standard eigenvalue problem for λ, it is of the form

$$L\hat{\phi} = \lambda M\hat{\phi}, \tag{17}$$

where L and M are differential operators. If we define the usual inner product

$$\langle \hat{\phi}_2, \hat{\phi}_1 \rangle = \int_{-1}^{1} \bar{\hat{\phi}}_2(y)\, \hat{\phi}_1(y)\, dy \tag{18}$$

on the manifold of twice differentiable complex-valued functions on $[-1, 1]$ which vanish together with their first derivatives at the end points, L and M are self-adjoint, and M is positive definite. Thus, if $(\hat{\phi}_1, \lambda_1)$ and $(\hat{\phi}_2, \lambda_2)$ are two eigenfunction/eigenvalue pairs of (17), we have

$$\lambda_1 \langle \hat{\phi}_2, M\hat{\phi}_1 \rangle = \langle \hat{\phi}_2, L\hat{\phi}_1 \rangle = \langle L\hat{\phi}_2, \hat{\phi}_1 \rangle = \bar{\lambda}_2 \langle M\hat{\phi}_2, \hat{\phi}_1 \rangle = \bar{\lambda}_2 \langle \hat{\phi}_2, M\hat{\phi}_1 \rangle. \tag{19}$$

Now setting $\hat{\phi}_1 = \hat{\phi}_2$, the positive definiteness of M implies that λ_1 is real while if $\hat{\phi}_1 \neq \hat{\phi}_2$ (19) implies that $\langle \hat{\phi}_2, M\hat{\phi}_1 \rangle = 0$. Thus, the eigenvalues are real and a pseudo-orthogonality condition exists which will permit easy evaluation of the coefficients in an eigenfunction expansion. Note too that in this case only one boundary condition at $x = 0$ has to be prescribed. Thus the eigenfunction expansion given explicitly by (8.1) and (8.2) is easy to obtain.

In view of the fact that for the full problem the expansion procedure is not obvious, we have chosen to try three procedures to expand a given initial-velocity field at $x = 0$. Let us assume that the eigenfunctions defined by (10) form a complete set and let us assume that $u^* = u(0, y)$ and $v^* = v(0, y)$, the velocity components at $x = 0$, are prescribed.

(i) Let $U_0(y)$ be the two-component vector, whose components are $u^*(y)$ and $v^*(y)$, the velocity components at $x = 0$,

$$U_0(y) = \begin{pmatrix} u^*(y) \\ v^*(y) \end{pmatrix}. \tag{20}$$

Now each eigenfunction $\phi_n(y, \lambda_n)$ of (10) leads to a velocity field with components $(u_n(y) \times e^{-\lambda_n x}, v_n(y) e^{-\lambda_n x})$.

Let

$$V_n(x,y) = \begin{pmatrix} u_n(y) \\ v_n(y) \end{pmatrix} e^{-\lambda_n x}. \tag{21}$$

The velocity field over the whole duct is then given by

$$U(x,y) = \sum_{n=1}^{\infty} a_n V_n(x,y) \tag{22}$$

which then has to yield the prescribed initial velocity at $x = 0$,

$$U_0(y) = \sum_{n=1}^{\infty} a_n V_n(0,y). \tag{23}$$

The first method used is to take a finite number of terms N on the right side of (23) and choose the coefficients such that

$$\| U_0(y) - \sum_{n=1}^{N} a_n V_n(0,y) \| \tag{24}$$

is a minimum. This amounts to being a least-error-squared fit over the initial data. The procedure naturally leads to a system of N linear algebraic equations for the coefficients $\{a_n, n = 1, 2 \ldots N\}$. If the eigenfunctions are complete, one would expect the a_n to tend to their limiting (correct) values, as $N \to \infty$. Table 2 shows the typical convergence behaviour of the a_n as N increases.

Table 2. The coefficients a_n ($n = 1, 2, \ldots, 10$) of the eigenfunction expansion for $R = 1, h = 0.5$, parabolic entry profile, as computed using (24) with $N = 10, 16, 22$.

	$N = 10$	$N = 16$	$N = 22$
a_1	$-4.37343 + 1.25242\,i$	$-4.436458 + 1.25025\,i$	$-4.3685 + 1.254\,i$
a_2	$-4.37343 - 1.25242\,i$	$-4.43645 - 1.25025\,i$	$-4.3685 - 1.254\,i$
a_3	$-2.5297 + 1.40461\,i$	$-2.53914 + 1.401\,i$	$-2.5376 + 1.39676\,i$
a_4	$-2.5297 - 1.40461\,i$	$-2.53914 - 1.401\,i$	$-2.5376 - 1.39676\,i$
a_5	$1.28629 + 0.31311\,i$	$1.3375 + 0.34886\,i$	$1.3331 + 0.35229\,i$
a_6	$1.28629 - 0.31311\,i$	$1.3375 - 0.34886\,i$	$1.3331 - 0.35229\,i$
a_7	$1.41788 - 0.65956\,i$	$1.47502 - 0.85422\,i$	$1.4622 - 0.85157\,i$
a_8	$1.41788 + 0.65956\,i$	$1.47502 + 0.85422\,i$	$1.4622 + 0.85157\,i$
a_9	$0.23783 - 0.30098\,i$	$-0.88791 - 0.3951\,i$	$-0.85169 - 0.40065\,i$
a_{10}	$0.23783 + 0.30098\,i$	$-0.88791 + 0.3951\,i$	$-0.85169 + 0.40065\,i$

(ii) The second method is based on the Schmidt orthonormalisation procedure used in Hilbert-space theory (Friedman [8]). We wish to use the vectors $\{V_n(0,y), n = 1, 2 \ldots\}$ given by (21) as a basis for the space of two-component vectors whose components are complex-valued functions on $[-1, 1]$. Define the inner product on this space by

$$\langle U, W \rangle = \int_{-1}^{1} (\bar{u}_1 w_1 + \bar{u}_2 w_2)\, dy, \tag{25}$$

where $U(y) = (u_1(y), u_2(y))$ and $W(y) = (w_1(y), w_2(y))$. With respect to this inner product

the V_n given by (21) are not an orthonormal set. We now generate from the set $\{V_n(x,y), n = 1, 2 \ldots\}$ a set $\{\hat{V}_n(x,y), n = 1, 2, \ldots\}$ which is orthonormal at $x = 0$ by the Schmidt-orthogonalisation procedure, as given for example in Friedman [8]. Since the $\hat{V}_n$ are linear combinations of the V_n they also satisfy the governing equations. If we then write

$$U(x,y) = \sum_{n=1}^{\infty} \hat{a}_n \hat{V}_n(x,y), \tag{26}$$

the coefficients $\hat{a}_n$ are now simply given by

$$\hat{a}_n = \langle U_0(y), \hat{V}_n(0,y) \rangle. \tag{27}$$

Thus, there is no need to solve even a system of equations once the orthonormal set of eigenfunctions is generated.

(iii) The third procedure depends on converting the non-standard eigenvalue problem (10) to a standard one by considering a system of equations. Defining τ and η to be the strain rates given by $\tau = u_x$ and $\eta = v_x$ and assuming modal solutions of the type $u(x,y) = \hat{u}(y) \exp(-\lambda x)$ etc., the governing equations can be written as

$$L\hat{W} = \lambda M\hat{W}, \tag{28}$$

where $\hat{W}$ is a 5-component vector

$$\hat{W}(y) = (\hat{u}(y), \hat{v}(y), \hat{p}(y), \hat{\tau}(y), \hat{\eta}(y)) \tag{29}$$

and L is a differential operator, and M is a constant matrix both of which are independent of λ,

$$L = \begin{bmatrix} -\frac{d^2}{dy^2} & 0 & 0 & R & 0 \\ 0 & -\frac{d^2}{dy^2} & \frac{d}{dy} & 0 & R \\ 0 & \frac{d}{dy} & 0 & 0 & 0 \\ 0 & 0 & 0 & 1 & 0 \\ 0 & 0 & 0 & 0 & 1 \end{bmatrix}, \quad M = \begin{bmatrix} 0 & 0 & 1 & -1 & 0 \\ 0 & 0 & 0 & 0 & -1 \\ 1 & 0 & 0 & 0 & 0 \\ -1 & 0 & 0 & 0 & 0 \\ 0 & -1 & 0 & 0 & 0 \end{bmatrix}. \tag{30}$$

Since (28) is now in standard form one can use the eigenfunctions of the adjoint L^* of L to expand a given 5-vector $\hat{W}_0(y)$ using a biorthogonality relation. However, since only u, v and ψ are known at $x = 0$, this procedure leads to an infinite system of algebraic equations for the coefficients $\hat{a}_n$ in an expansion of the form

$$\hat{W}(x, y) = \sum_{n=1}^{\infty} \hat{a}_n \hat{W}_n(y) \, e^{-\lambda_n x}. \tag{31}$$

This procedure is similar to the procedure used by Johnson and Little [9] to solve a problem in elastostatics.

The three procedures described above should serve to emphasise the unusual nature of the eigenfunction expansion. A single set of coefficients a_n in an expansion of the form $\psi = \Sigma a_n \phi_n(y) \, e^{-\lambda_n x}$ has to be determined by two conditions at $x = 0$. It is now clear that this rules out any direct orthogonality relation between the ϕ_n as then a single condition at $x = 0$ would determine the a_n. In contrast, the Appendix considers a related problem where direct orthogonality is possible.

Table 3. Comparison of the coefficients a_n of the eigenfunction expansion as obtained by the three methods (I) least-error-squared fit, (II) orthonormalisation and (III) reduction to standard form; $h = 0.5$, $R = 1000$.

Least error squared fit	Orthonormalisation	Reduction to standard form
0.2647	0.26412	0.26362
−0.03034	−0.030407	−0.03049
−0.01502	−0.015061	−0.015104
0.005611	0.005526	0.005522
0.003735	0.003684	0.003686
−0.001914	−0.001913	−0.001918
−0.001446	−0.001464	−0.001467
0.000967	0.000918	0.000921
0.0008	0.000773	0.000777
−0.000557	−0.000551	−0.000551

We have generally found that the three methods lead to almost the same answers, and therefore it appears that the expansion procedure is valid. Table 3 compares the coefficients given by the three methods for a typical case. Figure 7 shows the effectiveness of the eigenfunctions in representing a given initial parabolic profile over $0 \leqslant y \leqslant 0.5$. The representation would naturally be better if there were no discontinuity in the initial slope.

4.3 Results and discussion

All the calculations to be presented are for a symmetric sudden expansion with $h = 0.5$ and for a symmetric parabolic entry profile with zero v-velocity. The calculations utilised more than 20 terms in the eigenfunction-expansion procedure. It was found, generally, that the accuracy on the initial-velocity field representation increased with R; as for large R, more of the eigenvalues

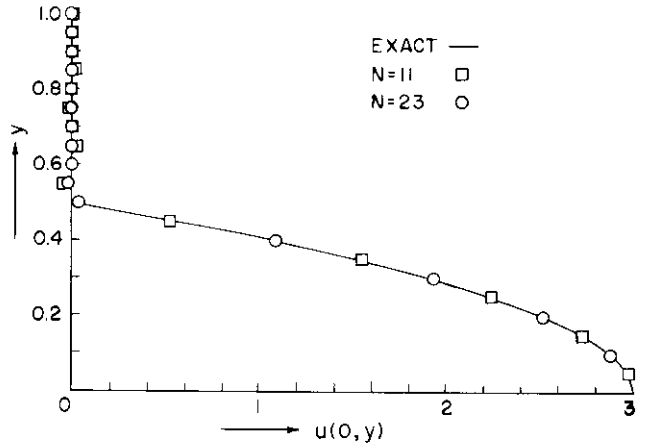

Figure 7. Representation of an initial profile at the duct entry, $u_0(y) = 3(1-4y^2)$ $(0 \leqslant y \leqslant 0.5)$, $u_0(y) = 0$ $(y > 0.5)$, $v_0(y) = 0$; $R = 100$.

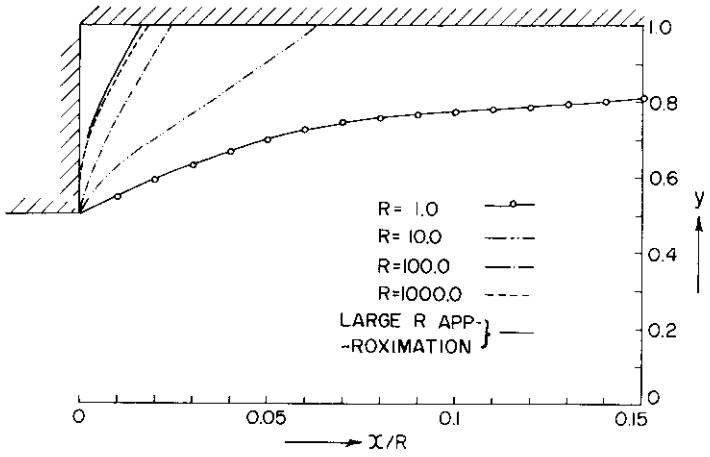

Figure 8. The shape of the separating streamline ($\Psi = 1$) for various values of the Reynolds number.

were real. In all cases, however, the order of the error was no worse than 0.01 on either $u_0(y)$ or $v_0(y)$.

Figure 8 shows the shape of the separating streamline, $\Psi = 1$, for various values of the Reynolds number. Also shown in this figure is the separating streamline as given by the large R approximation of Section 3. It is clear that as $R \to \infty$ the present solutions go smoothly to the large R solution. In fact the calculations for $R = 10\,000$ and $R = 100\,000$ are so close to the latter that they would be indistinguishable on the scale of Figure 8 and hence have not been shown.

It was pointed out in Section 3 that at high Reynolds numbers the Ψ-values were so close to unity in the separated flow region that, to the accuracy of the present computations, they could not be distinguished from unity. The situation is not so at lower Reynolds numbers. Figure 9 shows details of the recirculating region for $R = 1$. The Ψ- values depart sufficiently from 1 to be computable to the accuracy of the present calculations.

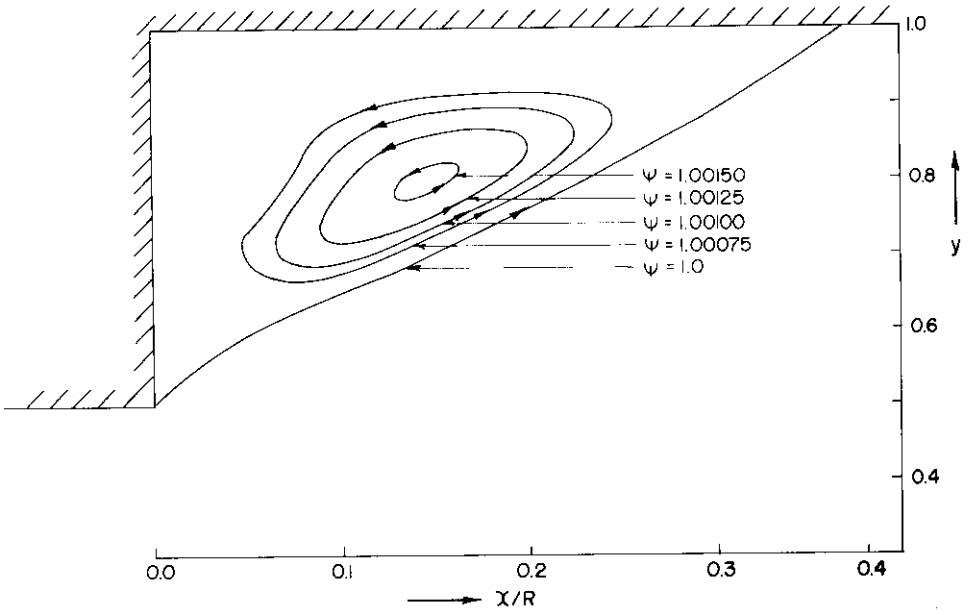

Figure 9. The recirculating region, $R = 1$.

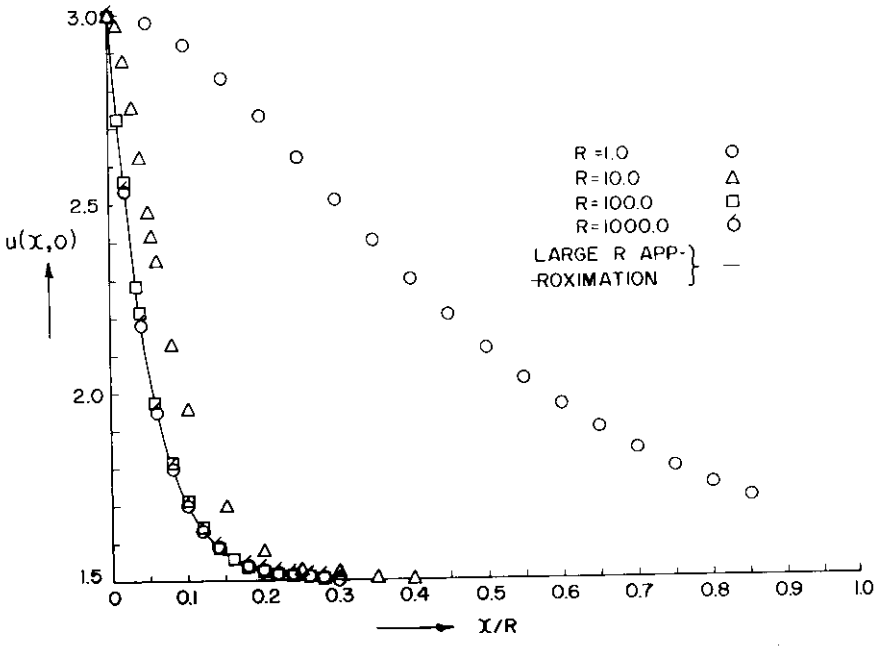

Figure 10. The centreline-velocity distribution.

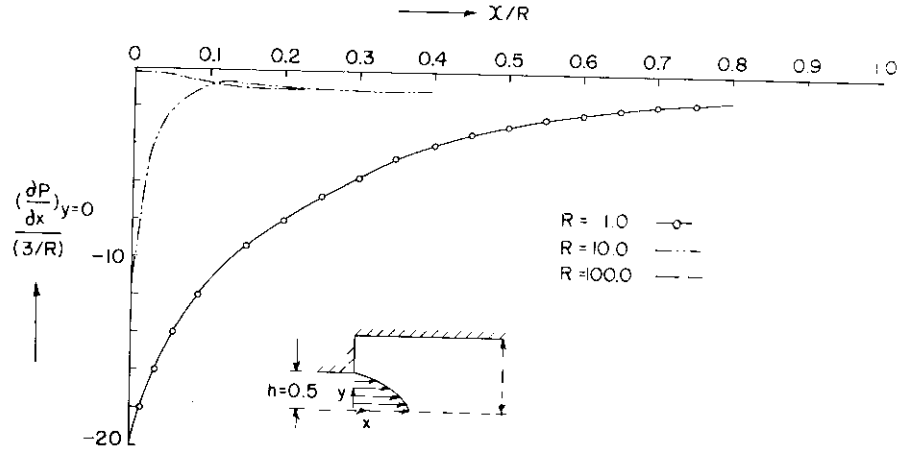

Figure 11. The centreline pressure gradient.

Figures 10 and 11 show the variation of the centreline axial velocity and centreline pressure gradient as functions of Reynolds number. It will be noted that at the lower Reynolds numbers, namely at R values of 1 and 10, the behaviour is quite different than that at the higher values, i.e. if x is scaled by R the approach to the Poiseuille flow is slower at the lower Reynolds numbers. One observes also that the pressure gradient near the entrance changes from large negative values to almost zero as the Reynolds number increases. Moreover, the pressure gradient is always negative for all x/R; this contrasts with Kumar and Yajnik, who found large positive values for $\partial p/\partial x$ near the duct entrance.

It is easy to establish from the x-momentum equation and the boundary conditions that at the side walls $\partial p/\partial x = R^{-1} u_{yy}$; thus if there is reverse flow at the walls $\partial p/\partial x$ has to be positive at the side walls. In the present case the velocities in the recirculating region are so small that the wall pressure gradient is extremely small, even if positive (note, of course, that Figure 11 shows the centreline pressure gradient and not the wall pressure gradient).

The length of the recirculating region, x_r, is shown in Figure 12 as a function of R. Clearly as $R \to \infty$, x_r/R approaches the value given by the large R approximation; for small Reynolds numbers, however, the dependence on R is significantly different. In fact, for large Reynolds numbers $x_r/R \simeq 0.017$ while for $R = 1$, $x_r/R \simeq 0.35$. Note also that this figure indicates that at least for the Oseen approximation, 46.6 (the Reynolds number of Hung and Macagno's calculation) would not be considered a sufficiently large Reynolds number for the high-Reynolds-number approximation to hold.

The validity of the high-Reynolds-number approximation is given considerable support by the results indicated in Figures 8–12. The hypotheses under which the approximation is derived appear to hold, and equally significant, the results of the full calculation merge smoothly into the results of Section 3 as $R \to \infty$. In fact, if one examines the coefficients of the full eigenfunction expansion for $R = 10^4$ and 10^5, it is found that these are virtually indistinguishable from the coefficients found in Section 3; since as $R \to \infty$ the eigenfunctions of Section 4 tend to those of Section 3, this constitutes a powerful vindication of the high-Reynolds-number approximation.

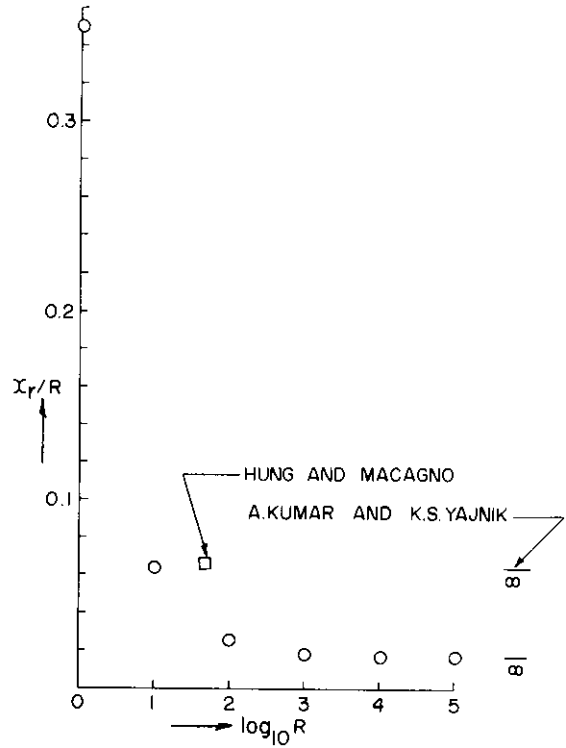

Figure 12. The length of the recirculating region as a function of R.

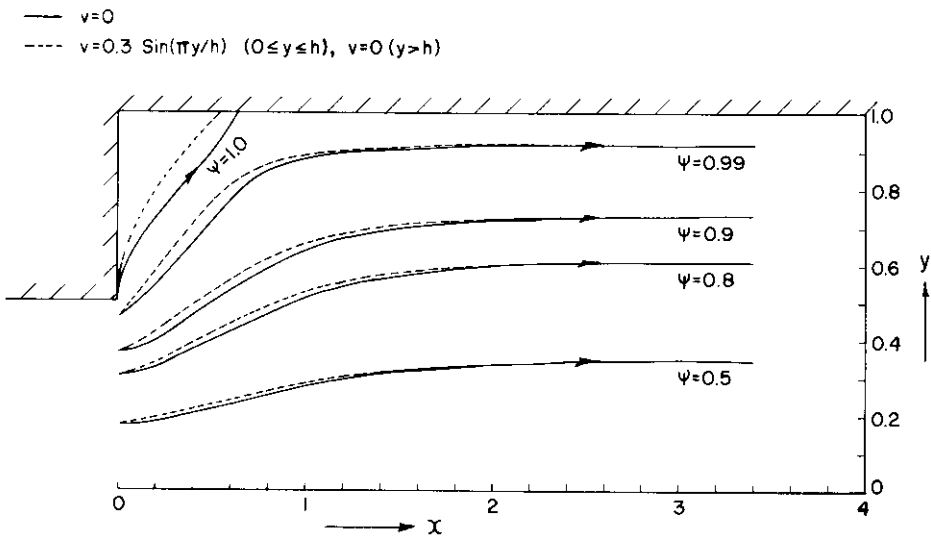

Figure 13. The streamline pattern when the initial v-velocity is given by $v = 0.3 \sin(\pi y/h)$ $(0 \leqslant y \leqslant h)$, $v = 0$ $(y > h)$; $R = 100$.

It is clear that the analysis can handle any given inlet velocity field. Figure 13 shows the streamline patterns for a case where the initial v-component is non-zero. We have in this section only considered symmetrical inlet flow fields. The methods used here easily extend to the general asymmetric case (cf. Figure 4), but then the antisymmetric eigenfunctions would also have to be considered. The corresponding eigenvalues satisfy the equation

$$\lambda \tan \lambda = \sqrt{R\lambda + \lambda^2} \tan \sqrt{R\lambda + \lambda^2}.$$

5. Conclusion

We have so far considered the flow field downstream of a sudden expansion in a duct. It is, interesting to compare this flow with the two-dimensional flow downstream of a baffle with an infinite number of holes of width 2a, whose adjacent centrelines are 2 units apart (Figure 14).

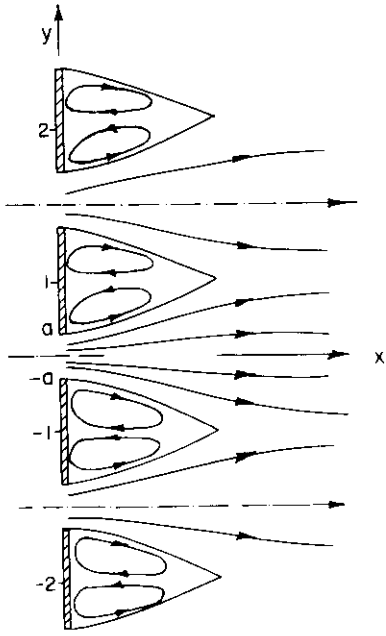

Figure 14. Two-dimensional flow past a baffle.

If one is given the u- and v- components of velocity at the plate, the model equations of Section 2 can be used to analyse the flow. One finds, as shown in the Appendix, that surprisingly the eigenvalues for this case are all real and the y-eigenfunctions are simply $\sin(n\pi y)$. The eigenvalues form two distinct sequences $\{n\pi\}$ and $\{(-R + \sqrt{R^2 + 4n^2\pi^2})/2\}$ and the coefficients in the eigenfunction expansion can be written down explicitly. The recirculating region again scales as R for large R. It is remarkable comparing the duct problem with the baffle problem that just the change of the side-wall conditions to periodic conditions in y leads to such differences in the analysis; real eigenvalues, explicit expansion procedure, etc. Though the operator is

the same, it acts on a different manifold of functions; this makes all the difference. For the duct problem it appears that the appropriate solution space is a Hilbert space whose elements are two-component vectors, each component being a function on $[-1, 1]$.

In conclusion we should like to state again the main features of the present work. It has been possible to solve a separated-flow problem using model equations over the whole range of Reynolds numbers. The analysis has led to an interesting study of a non-standard eigenvalue problem involving complex eigenvalues. And perhaps more significantly the analysis has shed some light on the limit equation used by Kumar and Yajnik, and the present results certainly support the essential validity of their ideas.

Finally it might be appropriate to indicate extensions to the present work that might be useful. From a fluid-mechanical point of view there would be real interest in considering the through-flow problem i.e. the flow in an infinitely long duct with a sudden expansion or flow through a baffle given the far-upstream velocity field. This would be a difficult problem, since the upstream scales are significantly different from the downstream scales, and an eigenfunction expansion procedure would require a difficult matching at $x = 0$. From a mathematical point of view it would be interesting to study the non-standard eigenvalue problem defined by (10); theorems on the eigenvalues, on expansion procedures and on completeness would be most useful. Work on a related, but simpler, problem in the theory of elasticity has been done recently by Gregory [10].

We would like to acknowledge the benefits of valuable discussions with our colleagues Dr. U.N. Sinha and Dr. A. Kumar. We are also grateful to Dr. A. Kumar for bringing to our notice the problem discussed in the Appendix.

Appendix

Consider the y-periodic flow field downstream of the baffle shown in Figure 14. Let $\Psi = y + \psi(x, y)$ and assume that the model equation (4) holds. The lateral boundary conditions are now

$$\psi(x, \pm 1) = \psi_{yy}(x, \pm 1) = 0.$$

Assume that $u_0(y)$ and $v_0(y)$ are given on $-1 \leqslant y \leqslant 1$ that they are symmetric and antisymmetric about $y = 0$ respectively and that $\int_0^1 u_0(\eta)\, d\eta = 1$. If we further assume that $\psi(x, y) = \sin(n\pi y) \exp(-\lambda x)$, the lateral boundary conditions are automatically satisfied and the governing equation forces λ to be given by

$$\lambda = \begin{cases} \pm n\pi \\ \dfrac{-R \pm \sqrt{R^2 + 4n^2\pi^2}}{2} \end{cases} \qquad n = 1, 2, 3, \ldots .$$

Now, if the eigenfunction expansion is taken in the form

$$\psi = \sum_{n=1}^{\infty} \{a_n e^{-n\pi x} + b_n e^{-(-R + \sqrt{R^2 + 4n^2\pi^2})\, x/2}\} \sin(n\pi y),$$

the coefficients are easily found to be given by

$$b_n = \frac{2\int_0^1 [\{u_0(y)-1\}\cos(n\pi y)+v_0(y)\sin(n\pi y)]\,dy}{[n\pi-\frac{1}{2}(-R+\{R^2+4n^2\pi^2\}^{1/2})]},$$

$$a_n = \frac{2}{n\pi}\int_0^1 \{u_0(y)-1\}\cos(n\pi y)\,dy - b_n.$$

References

[1] Chang, I. D., Navier-Stokes solutions at large distances from a finite body, *J. Math. Mech.* 10 (1961) 811–876.

[2] Oseen, C. W., *Neuere Methoden und Ergebnisse in der Hydrodynamik*, Akademiche Verlagsgesellschaft M. B. H., Leipzig 1927.

[3] Kusukawa, K., On the steady flow past an oblique flat plate at a high Reynolds number, *J. Phys. Soc. Japan* 29 (1970) 479–495.

[4] Miyagi, T., Oseen flow past a circular cylinder, *J. Phys. Soc. Japan* 37 (1974) 1699–1707.

[5] Hung, T. K. and Macagno, E. O., Laminar eddies in a two-dimensional conduit expansion, *La Houille Blanche* 21 (1966) 391–401.

[6] Kumar, A. and Yajnik, K. S., Internal separated flows at large Reynolds number, *J. Fluid Mech.* 97 (1980) 27–51.

[7] Dettman, J. W., *Applied complex variables*, Macmillan Co., 1965.

[8] Friedman, B., *Principles and techniques of applied mathematics*, J. Wiley & Sons, 1956.

[9] Johnson, M. W. and Little, R. W., The semi-infinite elastic strip, *Quart. Appl. Math.* 22 (1964) 335–344.

[10] Gregory, R. D., The traction boundary value problem for the elastostatic semi-infinite strip; existence of solution, and completeness of the Papkovich-Fadle eigenfunctions, *J. Elast.* 10 (1980) 295–327.